

# Venc Design and Velocity Estimation for Phase Contrast MRI

Shen Zhao, Rizwan Ahmad, and Lee C. Potter, *Senior Member, IEEE*

**Abstract**—In phase-contrast magnetic resonance imaging (PC-MRI), spin velocity contributes to the phase measured at each voxel. Estimation of velocity from potentially wrapped phase measurements is therefore the task of solving a system of noisy congruence equations. We propose *Phase Recovery from Multiple Wrapped Measurements* (PRoM) as a fast, approximate maximum likelihood estimator of velocity from multi-coil data with possible amplitude attenuation due to dephasing. The estimator can recover the fullest possible extent of unambiguous velocities, which can exceed four times the highest venc. The estimator uses all pairwise phase differences and the inherent correlations among them to minimize the estimation error. Derivation of the estimator yields explicit probabilities of unwrapping errors and the posterior probability distribution for the velocity estimate; this in turn allows for optimized design of the phase-encoded acquisition. Simulation, phantom, and in vivo results for three-point PC-MRI acquisitions validate the benefits of fast computation, reduced estimation error, increased recovered velocity range, and optimized acquisition. The examples presented demonstrate two orders of magnitude reduction in computational complexity and 10% decrease in root mean squared error versus conventional “dual-venc” techniques.

**Index Terms**—Phase-contrast MRI; dual-venc; phase unwrapping; congruence equations; sparse array design

## I. INTRODUCTION

PHASE-contrast magnetic resonance imaging (PC-MRI) is a quantitative, non-invasive technique to measure hemodynamics in vivo [1]. PC-MRI also enables higher dimensional velocimetry such as 4D flow imaging [2]. Spin velocity is encoded into voxel phase via a time-varying gradient field. Lowering the first moment of the encoding gradient extends the unaliased range but degrades the velocity-to-noise ratio (VNR). To address this issue, multi-point acquisitions such as “dual-venc” have been proposed, whereby a high-venc measurement is used to unwrap a potentially wrapped, but less noisy, low-venc velocity measurement [3], [4]. In contrast, multiple (possibly wrapped) pairwise phase differences can be jointly processed [5]–[7], leading to a potentially larger unambiguous range of velocities and a reduced estimation

error. Existing estimators usually employ a computationally expensive grid search and cannot guide the optimized design of the acquisition.

Building on our preliminary work [5], we propose *Phase Recovery from Multiple Wrapped Measurements* (PRoM), an approximate maximum likelihood estimator (MLE) for a set of linear congruence equations with additive correlated noise. The estimator is used in multi-point PC-MRI to jointly process all pairwise phase differences. The PRoM estimator first constructs a set of candidate tuples of wrapping integers. The probability that the true tuple of wrapping integers is in this set is arbitrarily close to 1. For each candidate tuple, the corresponding candidate velocity is found without grid searching as a simple weighted combination of the noisy measurements plus the candidate wrapping. The final velocity estimate is chosen among the small set of candidate velocities to maximize the likelihood function. The approximate MLE explicitly accommodates both intravoxel dephasing and the inherent noise correlation present among phase differences. Compared to simplified grid-search MLE, the computation of PRoM is orders of magnitude faster.

The probability distribution of the velocity estimate from noisy data is derived in closed form, which allows for the optimized design of the phase encoding. Additionally, the same estimation problem appears in other array processing applications, where PRoM extends current art [8], [9] to provide: a fast, grid-free estimator; accommodation of correlated noise; and, principled design of sparse array geometry. For validation, we have applied PRoM to data sets acquired from simulation, 1.5 T scan of a spinning phantom, and 3 T in vivo scan of a healthy volunteer.

## II. THEORY

### A. Phase Encoding

A time-varying magnetic gradient field may be used to encode spin velocity into image phase. Here, we consider encoding the velocity component in one direction. Consider a spin moving through a magnetic field; the Taylor series expansion of spin position  $p(t) \in \mathbb{R}$  at  $t = 0$  yields

$$p(t) = p(0) + \frac{v}{1!}t + \frac{a}{2!}t^2 + \dots, \quad (1)$$

where  $v$  is instantaneous velocity and  $a$  is acceleration. Let  $\gamma$  be the gyromagnetic ratio,  $B_0$  be the main static magnetic field strength, and  $g(t) \in \mathbb{R}$  be the time-varying magnetic field gradient. Then to first order approximation of  $p(t)$  [1],

This manuscript was submitted on September 10, 2021 and revised on February 17, 2022. This work was supported in part by NIH grants R01HL135489 and R01HL151697.

S. Zhao and L. Potter are with the Department of Electrical & Computer Engineering, Ohio State University, Columbus, OH 43210 USA (email: zhao.1758@osu.edu, potter.36@osu.edu).

R. Ahmad is with the Department of Biomedical Engineering, Ohio State University, Columbus, OH 43210 USA (email: ahmad.46@osu.edu).

the phase accumulated from  $t = 0$  to echo time TE is

$$\begin{aligned} \phi &= \int_0^{\text{TE}} \gamma(B_0 + g(t))p(t)dt \\ &\approx \underbrace{\gamma B_0 \text{TE} + \gamma p(0) \int_0^{\text{TE}} g(t)dt}_{\phi_0} + \underbrace{\gamma v \int_0^{\text{TE}} g(t)tdt}_{m_1} \\ &= \phi_0 + \gamma m_1 v, \end{aligned} \quad (2)$$

where  $m_0$  and  $m_1$  denote the zeroth and first moments of  $g(t)$ . The zeroth moment,  $m_0$ , encodes the spin position into phase and combines with  $\gamma B_0 \text{TE}$  to make the background phase,  $\phi_0$ . The first moment,  $m_1$ , encodes spin velocity into phase. So for  $N_e$ -point encoding and  $N_c$  coils, the integral of all spins in a voxel yields the measurement

$$\tilde{y}_{\alpha\beta} = A_\alpha S_\beta e^{i(\phi_0 + \gamma m_{1\alpha} v)} + \delta_{\alpha\beta}, \quad (3)$$

where  $\alpha \in \{1, \dots, N_e\}$  indexes over all encodings, and  $\beta \in \{1, \dots, N_c\}$  indexes over all coils. The resulting signal amplitudes are  $A_\alpha \in \mathbb{R}$ ;  $S_\beta \in \mathbb{C}$  is the coil sensitivity weight;  $v$  is the resultant instantaneous velocity;  $m_{1\alpha} \in \mathbb{R}$  is the first moment;  $\delta_{\alpha\beta} \in \mathbb{C}$  is independent and identically distributed (i.i.d.) complex circularly symmetric Gaussian noise. This i.i.d. assumption can be aided by pre-whitening along the coil dimension. The existence of heterogeneous spin velocities and proton density can make  $v$  in (3) differ from the mean moving spin velocity (e.g. partial volume effect) and can reduce the amplitude (e.g. intravoxel dephasing effect). Generally,  $A_\alpha$  decreases as  $|m_{1\alpha}|$  increases [10].

Let  $\tilde{\mathbf{Y}}$  denote an  $N_e \times N_c$  complex-valued measurement matrix with  $(\alpha, \beta)^{\text{th}}$  entry  $\tilde{y}_{\alpha\beta}$ , and observe that the unambiguous range of velocities for the  $N_e$  encodings is

$$\Omega' = \text{LCM} \left( \frac{2\pi}{\gamma m_{11}}, \dots, \frac{2\pi}{\gamma m_{1N_e}} \right), \quad (4)$$

where  $\text{LCM}(\cdot)$  denotes least common multiple, which is the smallest positive real number that is an integer multiple of all input numbers. It follows that  $v$  and  $v + \Omega'$  are indistinguishable given data,  $\tilde{\mathbf{Y}}$ . Considering noise, the MLE of  $v$  involves  $N_e + N_c + 2$  unknowns,  $\{v, \phi_0, A_1, \dots, A_{N_e}, S_1, \dots, S_{N_c}\}$ , and is a nonlinear least-squares fit to the data. The optimization task can be reduced to

$$\underset{\mathbf{s}}{\text{argmax}} \frac{\mathbf{s}^H \tilde{\mathbf{R}} \mathbf{s}}{\mathbf{s}^H \mathbf{s}} \quad \text{s.t. } \|\mathbf{s}\| = 1, \quad (5)$$

where  $\tilde{\mathbf{R}} \in \mathbb{C}^{N_e \times N_e}$  and the ‘‘steering vector’’  $\mathbf{s} \in \mathbb{C}^{N_e \times 1}$  are

$$\begin{aligned} \tilde{\mathbf{R}} &= \tilde{\mathbf{Y}} \tilde{\mathbf{Y}}^H \\ \mathbf{s} &= [A_1 e^{i\gamma m_{11} v}, \dots, A_{N_e} e^{i\gamma m_{1N_e} v}]^T. \end{aligned} \quad (6)$$

Derivation of (5) is a straightforward extension of [11, p. 288] to accommodate unequal amplitudes,  $A_\alpha$ . Here,  $(\cdot)^T$  and  $(\cdot)^H$  denotes transpose, and conjugate transpose. The steering vector  $\mathbf{s}$  is determined up to scale. For a given  $v$ , the amplitudes may be found by solving (5) as a generalized eigenvalue problem [12, p.461]; yet, the optimization over  $v$  nonetheless encounters a difficult cost surface with many

local minima. A simple illustration of the sum of squared error versus velocity using a single-coil, symmetric three-point acquisition is shown in Fig. 1. Data are simulated using  $\left[ \frac{|A_1 S_1|}{\sigma(\delta_{11})}, \frac{|A_2 S_1|}{\sigma(\delta_{21})}, \frac{|A_3 S_1|}{\sigma(\delta_{31})} \right] = [2.5, 5, 2.5]$  to represent a moderate 50% loss of signal amplitude due to intravoxel dephasing. Throughout the paper, we use same 50% in simulation. The fit error at the true velocity,  $v = 0$  cm/s, is shown by the red diamond, and the global minimum at  $v \approx -1.01$  cm/s for the given noise realization is shown by the green marker. Competing local minima, shown as blue markers, may become the global minimum due to noise, thereby causing unwrapping errors.

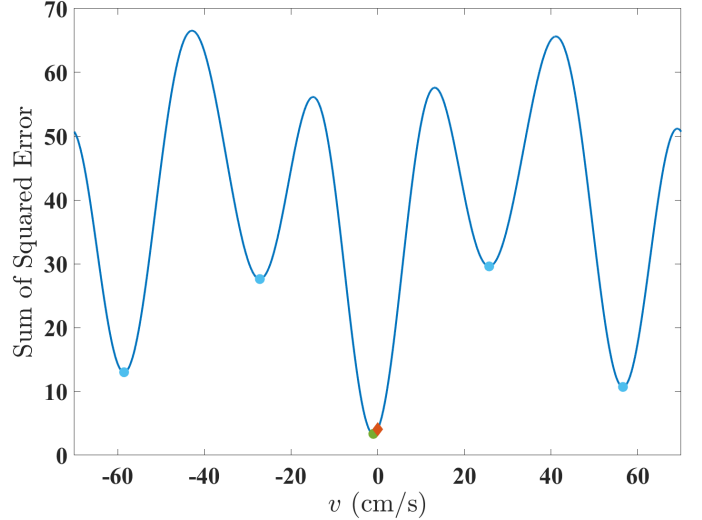


Fig. 1. Sum of squared error versus velocity for a single coil, symmetric three-point acquisition.  $\gamma[m_{11}, m_{12}, m_{13}] = [-\frac{\pi}{20}, \frac{\pi}{70}, \frac{\pi}{20}]$  s/cm,  $\left[ \frac{|A_1 S_1|}{\sigma(\delta_{11})}, \frac{|A_2 S_1|}{\sigma(\delta_{21})}, \frac{|A_3 S_1|}{\sigma(\delta_{31})} \right] = [2.5, 5, 2.5]$ . The fit error to the noisy data at the true velocity  $v = 0$  cm/s is shown by the red diamond. The global minimum at  $v \approx -1.01$  cm/s for the given noise realization is shown by the green marker. Competing local minima, shown as light blue markers, may become the global minimum due to noise, thereby causing unwrapping errors.

## B. Estimation of Phase Noise Covariance

From (5) we see that the  $\tilde{\mathbf{R}}$  is a sufficient statistic for  $v$  in (3). We depart from the multi-variate optimization in (5) to instead work with the phases of the off-diagonal entries of  $\tilde{\mathbf{R}}$ , and we use amplitudes of  $\tilde{\mathbf{Y}}$  to inform the phase-to-noise ratio. In so doing, we gain four advantages: (1) fast, grid-free parameter estimator for velocity,  $v$ ; (2) characterization of the unambiguous set of estimated velocities; (3) characterization of the probability of unwrapping errors; (4) ability to design the encodings  $[m_{11}, \dots, m_{1N_e}]$  to minimize mean squared estimation error subject to guarantees on the probability of unwrapping error and required unambiguous range. Further, the proposed surrogate estimator is asymptotically efficient, providing a very good approximation to the MLE. In this section, we derive an approximate covariance matrix for the phase measurements in  $\tilde{\mathbf{R}}$  to lay the groundwork for building the proposed estimator of  $v$ .

Observe that  $\tilde{\mathbf{R}} = \tilde{\mathbf{Y}}\tilde{\mathbf{Y}}^H$  performs coil combining and phase differencing. Denote the  $(a, b)$ <sup>th</sup> entry of  $\tilde{\mathbf{R}}$  as  $\tilde{r}_{ab}$ , so

$$\tilde{r}_{ab} = \sum_{\beta} \tilde{y}_{a\beta} \tilde{y}_{b\beta}^*, \quad (7)$$

where  $(\cdot)^*$  denotes complex conjugation. The noisy phase difference  $\tilde{\theta}_{ab}$  for encodings  $a > b \in \{1, \dots, N_e\}$  is

$$\tilde{\theta}_{ab} = \angle \tilde{r}_{ab}, \quad (8)$$

where  $\angle(\cdot)$  denotes angle of a complex number. This phase differencing results in venc value

$$\text{venc}_{ab} = \frac{\pi}{\gamma(m_{1a} - m_{1b})}. \quad (9)$$

We have  $\frac{N_e(N_e-1)}{2}$  such combinations. Throughout the paper, we let  $\text{venc}_{ab}$  have units cm/s. Multiplying the vencs with phases, we obtain a (possibly wrapped) noisy velocity  $\tilde{v}_{ab}$

$$\tilde{v}_{ab} = \frac{\tilde{\theta}_{ab}}{\pi} \text{venc}_{ab}. \quad (10)$$

Phases  $\tilde{\theta}_{ab}$  are unambiguous on any interval of length  $2\pi$ , and for convenience we use  $[0, 2\pi)$ ; so,  $\tilde{v}_{ab} \in [0, 2\text{venc}_{ab})$ . Thus, we have a set of noisy congruence equations for  $v$ :

$$\tilde{v}_{ab} \equiv v + n_{ab} \pmod{2\text{venc}_{ab}}, \quad (11)$$

where  $n_{ab}$  is additive zero mean noise. Define  $k_{ab}$  as the wrapping integer for  $\tilde{v}_{ab}$ . Momentarily assume that the true wrapping integer,  $k_{ab}$ , is known; then, we can rewrite (11) as a set of linear equations:

$$\tilde{\mathbf{v}} + \mathbf{k} \circ 2\mathbf{venc} = v\mathbf{1} + \mathbf{n}, \quad (12)$$

where  $\circ$  is the Hadamard (element-wise) product and

$$\begin{aligned} \tilde{\mathbf{v}} &= [\tilde{v}_{21}, \dots, \tilde{v}_{N_e(N_e-1)}]^\top \\ \mathbf{k} &= [k_{21}, \dots, k_{N_e(N_e-1)}]^\top \\ \mathbf{venc} &= [\text{venc}_{21}, \dots, \text{venc}_{N_e(N_e-1)}]^\top \\ \mathbf{1} &= [1, \dots, 1]^\top \\ \mathbf{n} &= [n_{21}, \dots, n_{N_e(N_e-1)}]^\top. \end{aligned} \quad (13)$$

From the Chinese remainder theorem, the smallest  $\Omega > 0$  such that  $v + \Omega$  satisfies (11) is

$$\Omega = \text{LCM}(2\mathbf{venc}). \quad (14)$$

This also implies that  $\Omega$  is the smallest repetition period of  $v$  to construct the same  $\tilde{\mathbf{R}}$ . Recall from (4) that  $\Omega'$  is a repetition period of  $v$  to construct the same  $\tilde{\mathbf{Y}}$ , as well as the same  $\tilde{\mathbf{R}}$ . So,  $\Omega'$  is an integer multiple of  $\Omega$ .

Similar to the assumption  $\tilde{\theta}_{ab} \in [0, 2\pi)$ , we assume  $v \in [0, \Omega)$  for convenience of derivation. This interval could also be shifted to  $[-\frac{\Omega}{2}, \frac{\Omega}{2})$ , for example, for bidirectional flow in MRI.

Let  $\hat{v} \in [0, \Omega)$  be the linear unbiased estimator of  $v$  with smallest root mean squared error (RMSE). To compute  $\hat{v}$  from the noisy  $\tilde{\mathbf{v}}$  in (12), we only need the covariance matrix of the noise in the remainders,  $\Sigma(\mathbf{n})$ . Define  $\sigma$  to be the standard

deviation of the i.i.d. noise  $\delta_{\alpha\beta}$  in (3). The mean and variance of  $\tilde{r}_{ab}$  are [13]:

$$\mathbb{E}(\tilde{r}_{ab}) = \sum_{\beta} A_a A_b e^{i\gamma(m_{1a} - m_{1b})v} |S_{\beta}|^2 \quad (15)$$

$$\sigma^2(\tilde{r}_{ab}) = \sum_{\beta} (\sigma^2(A_a^2 + A_b^2) |S_{\beta}|^2 + \sigma^4). \quad (16)$$

Then from (15)-(16), the squared signal-to-noise ratio (SNR), or Rician factor, for  $\tilde{r}_{ab}$  is

$$\begin{aligned} \text{SNR}^2(\tilde{r}_{ab}) &= \frac{|\mathbb{E}(\tilde{r}_{ab})|^2}{\sigma^2(\tilde{r}_{ab})} \\ &= \frac{\left(\sum_{\beta} A_a A_b |S_{\beta}|^2\right)^2}{\sum_{\beta} (\sigma^2(A_a^2 + A_b^2) |S_{\beta}|^2 + \sigma^4)} \\ &= \frac{\left(\sum_{\beta} s_{a\beta} s_{b\beta}\right)^2}{\sum_{\beta} (s_{a\beta}^2 + s_{b\beta}^2 + 1)}, \end{aligned} \quad (17)$$

where  $s_{\alpha\beta} = \frac{|A_{\alpha} S_{\beta}|}{\sigma} = \text{SNR}(\tilde{y}_{\alpha\beta})$ . As  $\text{SNR}(\tilde{r}_{ab}) \rightarrow \infty$ ,  $\tilde{\theta}_{ab}$  converges in distribution to a Gaussian random variable. On the contrary, as  $\text{SNR}(\tilde{r}_{ab}) \rightarrow 0$ ,  $\tilde{\theta}_{ab}$  converges in distribution to a uniformly distributed random variable on  $[0, 2\pi)$ . Because  $\lim_{x \rightarrow 0} \frac{x}{\sin(x)} = 1$ , and  $\sigma(\tilde{\theta}_{ab})$  conditioned on no wrapping is inversely proportional to  $\text{SNR}(\tilde{r}_{ab})$ ,

$$\sigma^2(\tilde{\theta}_{ab}) \approx \frac{1}{2 \text{SNR}^2(\tilde{r}_{ab})} = \frac{\sum_{\beta} (s_{a\beta}^2 + s_{b\beta}^2 + 1)}{2 \left(\sum_{\beta} s_{a\beta} s_{b\beta}\right)^2}. \quad (18)$$

Similarly, we can obtain covariance given no wrapping

$$\begin{aligned} \text{cov}(\tilde{\theta}_{ab}, \tilde{\theta}_{cb}) &\approx \frac{|\text{cov}(\tilde{r}_{ab}, \tilde{r}_{cb})|}{\sum_{\beta} 2A_a A_b^2 A_c |S_{\beta}|^4} = \frac{N_c}{\sum_{\beta} 2s_{b\beta}^2} \\ \text{cov}(\tilde{\theta}_{ab}, \tilde{\theta}_{bd}) &\approx \frac{-N_c}{\sum_{\beta} 2s_{b\beta}^2} \end{aligned} \quad (19)$$

and  $\text{cov}(\tilde{\theta}_{ab}, \tilde{\theta}_{cd}) = 0$  for two phase differences that do not share a common encoding.

In practice, it may be difficult to accurately estimate the noise power for each voxel, and thus hard to estimate  $s_{\alpha\beta}$ . To ameliorate estimation difficulty and use complex measurements  $\tilde{y}_{\alpha\beta}$  only, we further approximate and scale the variance and covariance:

$$\sigma^2(\tilde{\theta}_{ab}) \approx \frac{\sum_{\beta} (s_{a\beta}^2 + s_{b\beta}^2)}{2 \left(\sum_{\beta} s_{a\beta} s_{b\beta}\right)^2} \propto \frac{\sum_{\beta} (|\tilde{y}_{a\beta}|^2 + |\tilde{y}_{b\beta}|^2)}{2 \left(\sum_{\beta} |\tilde{y}_{a\beta}| |\tilde{y}_{b\beta}|\right)^2} \quad (20)$$

$$\text{cov}(\tilde{\theta}_{ab}, \tilde{\theta}_{cb}) \propto \frac{N_c}{\sum_{\beta} 2|\tilde{y}_{b\beta}|^2}, \quad (21)$$

where  $\propto$  denotes ‘‘approximately proportional to.’’ Here, the scaling factors are the same for (20) and (21). Let

$$\tilde{\boldsymbol{\theta}} = [\tilde{\theta}_{21}, \dots, \tilde{\theta}_{N_e(N_e-1)}]^\top.$$

Then, with the elementwise approximations above, we can formulate the scaled approximated  $\Sigma(\tilde{\boldsymbol{\theta}})$  directly from observed pixel magnitudes. This scaling does not affect the estimator  $\hat{v}$ ,

as seen from (30) below. Finally, because the true covariance matrix is close to rank deficient, the element-wise approximations in (20) and (21) can potentially violate the positive semi-definite property of a covariance matrix. Accordingly, we follow the approximation step by projection to the closest positive semi-definite matrix [14]. This projection operator,  $\Pi(\cdot)$ , for a symmetric matrix  $\mathbf{M}$  with eigen-decomposition  $\mathbf{M} = \mathbf{V}\mathbf{S}\mathbf{V}^{-1}$  is given by

$$\Pi(\mathbf{M}) = \mathbf{V} \max(\mathbf{S}, 0) \mathbf{V}^{-1}, \quad (22)$$

where  $\max(\mathbf{S}, 0)$  is applied element-wise to the eigenvalues.

To illustrate accuracy of covariance modeling, we adopt the cosine similarity metric, which is scale invariant. For modeled covariance  $\Pi(\Sigma(\tilde{\theta}))$  and sample covariance  $\tilde{\Sigma}(\theta)$ , the cosine similarity is

$$\frac{\text{Trace}\left(\Pi(\Sigma(\tilde{\theta}))^H \tilde{\Sigma}(\theta)\right)}{\left\|\Pi(\Sigma(\tilde{\theta}))\right\|_F \left\|\tilde{\Sigma}(\theta)\right\|_F}. \quad (23)$$

Results are computed for the case of a single-coil, symmetric encoding, and intravoxel dephasing  $2s_{11} = s_{21} = 2s_{31}$ ;  $10^6$  random draws are used at each  $s_{21}$  to provide a low-variance sample covariance matrix and to compute the mean cosine similarity. Fig. 2 displays the similarity metric results, from which we see excellent agreement for  $s_{21} > 2$ . Thus, the covariance model is accurate at modest SNR. Also shown in Fig. 2 is the similarity metric for the (scaled) identity covariance model, which is implicitly employed when using least-squares estimation with phase differences [7].

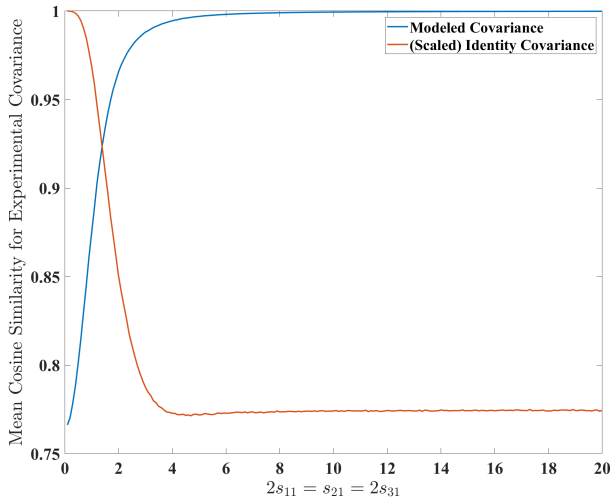


Fig. 2. Mean cosine similarity for the modeled covariance matrix versus experimental covariance using  $10^6$  trials at each  $s_{21}$  value for single coil and  $2s_{11} = s_{21} = 2s_{31}$ .

From (10), the wrapped velocity measurements are linearly related to the phase differences; thus, the approximated scaled positive semi-definite covariance matrix for the noise,  $\mathbf{n}$ , in (12) conditioned on no wrapping is

$$\Sigma(\mathbf{n}) \approx \frac{1}{\pi^2} \text{diag}(\mathbf{venc}) \Pi(\Sigma(\tilde{\theta})) \text{diag}(\mathbf{venc}). \quad (24)$$

### C. Best Linear Unbiased Estimator

Based on the covariance derivation in II-B, we can now formulate the estimator. We adopt two approximations suitable when the SNR is not extremely low. Our first approximation is that  $\mathbf{n}$  follows a joint Gaussian distribution with covariance matrix given in (24),

$$\mathbf{n} \sim \mathcal{N}(0, \Sigma(\mathbf{n})). \quad (25)$$

Denote the velocity estimate  $\hat{v}$  given wrapping integers  $\mathbf{k}$  as  $\hat{v}_{\mathbf{k}}$ . Then, due to (25),  $\hat{v}_{\mathbf{k}}$  and its resulting RMSE given no wrapping,  $\sigma(\hat{v}_{\mathbf{k}})$ , are

$$\hat{v}_{\mathbf{k}} = \langle \mathbf{w}^T (\tilde{v} + \mathbf{k} \circ 2\mathbf{venc}) \rangle_{\Omega} \quad (26)$$

$$\sigma(\hat{v}_{\mathbf{k}}) = \mathbf{w}^T \Sigma(\mathbf{n}) \mathbf{w}, \quad (27)$$

where

$$\mathbf{w}^T = \frac{\mathbf{1}^T \Sigma^{-1}(\mathbf{n})}{\mathbf{1}^T \Sigma^{-1}(\mathbf{n}) \mathbf{1}}, \quad (28)$$

and  $\langle a \rangle_b$  denotes remainders after elementwise modulo  $\mathbf{a}$  by  $\mathbf{b}$ . Thus, the estimate  $\hat{v}_{\mathbf{k}}$  is a weighted sum of unwrapped noisy velocities.

The second assumption we adopt is

$$\mathbb{P}(-\mathbf{venc} \preceq \mathbf{n} \preceq \mathbf{venc}) \approx 1, \quad (29)$$

where  $\preceq$  is element-wise less than or equal. This approximation yields the likelihood  $\mathbb{P}(\tilde{v}|v)$

$$\mathbb{P}(\tilde{v}|v) \approx \frac{e^{-\frac{1}{2} d_{2\mathbf{venc}}^T(\tilde{v}, v\mathbf{1}) \Sigma^{-1}(\mathbf{n}) d_{2\mathbf{venc}}(\tilde{v}, v\mathbf{1})}}{\det(2\pi \Sigma^{-1}(\mathbf{n}))} \quad (30)$$

where  $d_z(\mathbf{x}, \mathbf{y})$  is a “wrapped displacement” between  $\mathbf{x}$  and  $\mathbf{y}$  with respect to  $\mathbf{z}$ ,

$$d_z(\mathbf{x}, \mathbf{y}) \triangleq \mathbf{x} - \mathbf{y} - \text{round}((\mathbf{x} - \mathbf{y}) \oslash \mathbf{z}) \circ \mathbf{z}, \quad (31)$$

with  $\oslash$  denoting elementwise division. One could perform search over all possible  $\mathbf{k}$  to minimize the negative log likelihood,

$$\mathcal{L}(\tilde{v}, \hat{v}_{\mathbf{k}}) = \frac{1}{2} d_{2\mathbf{venc}}^T(\tilde{v}, \hat{v}_{\mathbf{k}}\mathbf{1}) \Sigma^{-1}(\mathbf{n}) d_{2\mathbf{venc}}(\tilde{v}, \hat{v}_{\mathbf{k}}\mathbf{1}). \quad (32)$$

In II-D, we instead present a fast method to detect the best wrapping integers,  $\mathbf{k}^*$ . In II-F and II-H, we explicitly consider three-point encoding,  $N_e = 3$ , to provide concrete results and to optimize the design of  $\mathbf{venc}$  and underlying first moments.

### D. PRoM

We introduce a fast estimator based on (26) and detection of the wrapping integers,  $\mathbf{k}$ . We refer to this detector and (26) together as *Phase Recovery from Multiple Wrapped Measurements* (PRoM). PRoM extends the prior signal processing result in [15] to accommodate correlated phase errors and to provide a fast computation of the wrapping integers. Moreover, PRoM provides a grid-free alternative to grid search over  $v$ .

Assuming  $v \in [0, \Omega)$ , define the set  $\mathcal{K}'(\tilde{v})$  of wrapping integers

$$\mathcal{K}'(\tilde{v}) = \{\mathbf{k} | -\mathbf{1} \preceq \mathbf{k} \preceq \mathbf{h}\} \quad (33)$$

$$\mathbf{h} = \Omega\mathbf{1} \oslash 2\mathbf{venc}. \quad (34)$$

By (29),  $\mathbb{P}(\mathbf{k} \in \mathcal{K}'(\tilde{\mathbf{v}})) \approx 1$ . So, from (26) and (30), we can minimize the negative log likelihood

$$\hat{v} = \underset{v \in [0, \Omega]}{\operatorname{argmin}} \mathcal{L}(\tilde{\mathbf{v}}, v) = \underset{v \in \{\hat{v}_{\mathbf{k}} | \mathbf{k} \in \mathcal{K}'(\tilde{\mathbf{v}})\}}{\operatorname{argmin}} \mathcal{L}(\tilde{\mathbf{v}}, v), \quad (35)$$

with probability  $\approx 1$ . Next, we use two steps to decrease the cardinality of  $\mathcal{K}'(\tilde{\mathbf{v}})$ , denoted as  $|\mathcal{K}'(\tilde{\mathbf{v}})|$ . First, since  $\mathbf{w}^\top \mathbf{1} = 1$  by (28) and  $\mathbf{h} \circ 2\mathbf{venc} = \Omega \mathbf{1}$  by (34), we have

$$\langle \mathbf{w}^\top (\tilde{\mathbf{v}} + \mathbf{k} \circ 2\mathbf{venc}) \rangle_\Omega = \langle \mathbf{w}^\top (\tilde{\mathbf{v}} + (\mathbf{k} + \mathbf{h}) \circ 2\mathbf{venc}) \rangle_\Omega, \quad (36)$$

i.e.,  $\hat{v}_{\mathbf{k}} = \hat{v}_{\mathbf{k}+\mathbf{h}}$ . Second, leveraging the equality constraint in (12) and invoking the second approximation in (29), we have

$$\mathbb{P}\left(-\frac{1}{2} \preceq \mathbf{k} + (\tilde{\mathbf{v}} - v\mathbf{1}) \circ (2\mathbf{venc}) \preceq \frac{1}{2}\right) \approx 1. \quad (37)$$

Combining the two steps above, the pruned search set for  $\mathbf{k}$  can be expressed

$$\mathcal{K}(\tilde{\mathbf{v}}) = \left\{ \mathbf{k} \mid -\frac{1}{2} \preceq \mathbf{k} + (\tilde{\mathbf{v}} - v\mathbf{1}) \circ (2\mathbf{venc}) \preceq \frac{1}{2}, \right. \\ \left. v \in [0, \Omega), -\mathbf{1} \preceq \mathbf{k} - \mathbf{h} \right\}. \quad (38)$$

Thus, the minimization in (35) can be further reduced to

$$\hat{v} = \underset{v \in \{\hat{v}_{\mathbf{k}} | \mathbf{k} \in \mathcal{K}(\tilde{\mathbf{v}})\}}{\operatorname{argmin}} \mathcal{L}(\tilde{\mathbf{v}}, v), \quad (39)$$

with probability  $\approx 1$ . Together, the construction of the pruned set,  $\mathcal{K}(\tilde{\mathbf{v}})$ , of candidate wrapping integers and the efficient search over  $\{\hat{v}_{\mathbf{k}} | \mathbf{k} \in \mathcal{K}(\tilde{\mathbf{v}})\}$  to minimize  $\mathcal{L}(\tilde{\mathbf{v}}, v)$  comprise PRoM, an approximate MLE of  $v$ . For a general  $N_e$ -point encoding, PRoM pseudo-code is given in Alg. 1, and PRoM code is available at <https://github.com/Zhao-Shen/PRoM>.

---

#### Algorithm 1 PRoM for $N_e$ -point Encoding

---

**Require:** Measurements,  $\tilde{\mathbf{Y}}$ . First moments,  $m_{11}, \dots, m_{1N_e}$ .

- 1: Calculate  $\mathbf{venc}, \tilde{\mathbf{v}}, \Omega, \mathcal{K}(\tilde{\mathbf{v}})$  via (9, 11, 14, 38).
- 2: Calculate scaled  $\Sigma(\mathbf{n})$  and  $\mathbf{w}$  via (24, 28).
- 3: Calculate  $\hat{v}$  via (26, 39).

**Ensure:**  $\hat{v}$

---

Fig. 3 illustrates  $\mathcal{L}(\tilde{\mathbf{v}}, \hat{v})$  for  $\mathbf{venc} = [35, 10, 14]^\top$  cm/s. The searched candidates  $\{\hat{v}_{\mathbf{k}} | \mathbf{k} \in \mathcal{K}(\tilde{\mathbf{v}})\}$  are marked by superimposed red dots. For this case,  $|\mathcal{K}'(\tilde{\mathbf{v}})| = 252$  and  $|\mathcal{K}(\tilde{\mathbf{v}})| = 14$ ; thus, 94% of the search space  $\mathcal{K}'$  is bypassed via the proposed construction of  $\mathcal{K}(\tilde{\mathbf{v}})$ . If  $\mathbf{n}$  is known to concentrate in a smaller volume compared to the second assumption (29), or  $v$  is known and restricted to a range less than  $\Omega$ , then  $\mathcal{K}(\tilde{\mathbf{v}})$  may be further pruned accordingly.

To illustrate the reduction of computation complexity in PRoM, consider the case in Fig. 3. Grid search MLE over velocity with spacing used in [7] entails computation for 7000 candidate velocities. In contrast, PRoM only requires search over only  $|\mathcal{K}(\tilde{\mathbf{v}})| = 14$  candidates, yielding a 500-times reduction.

PRoM admits a simple geometric interpretation. Observe that the noisy velocity measurement  $\tilde{\mathbf{v}}$  resides in a hyper-rectangle  $\{\tilde{\mathbf{v}} | \mathbf{0} \preceq \tilde{\mathbf{v}} \preceq 2\mathbf{venc}\}$ . The vector of noiseless velocity

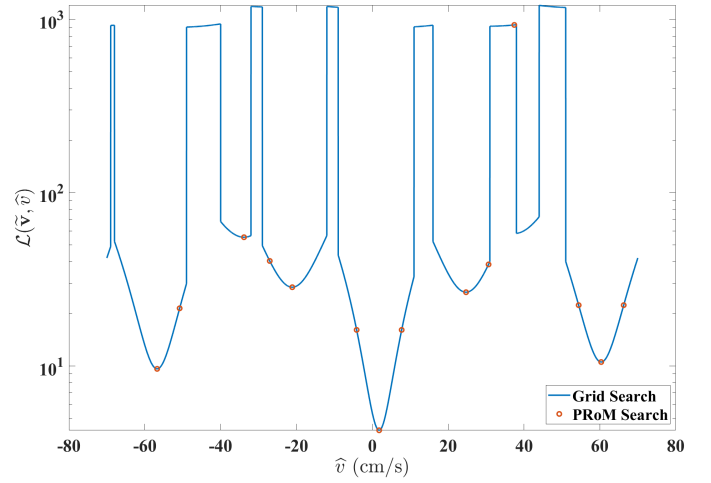


Fig. 3. Negative log likelihood  $\mathcal{L}(\tilde{\mathbf{v}}, \hat{v})$ , for single coil, symmetric three-point encoding,  $\tilde{\mathbf{v}} = [3, 1, 2]^\top$  cm/s,  $\mathbf{venc} = [35, 10, 14]^\top$  cm/s,  $[\mathbf{s}_{11}, \mathbf{s}_{21}, \mathbf{s}_{31}] = [2.5, 5, 2.5]$ . The red dots mark the PRoM searched candidates  $\{\hat{v}_{\mathbf{k}} | \mathbf{k} \in \mathcal{K}(\tilde{\mathbf{v}})\}$ .

measurements  $\langle v\mathbf{1} \rangle_{2\mathbf{venc}}$  for  $v \in [0, \Omega)$  is a point in the hyper-rectangle lying on wrapped line segments parallel to  $\mathbf{1}$ . Then,  $\hat{v}$  is found by an oblique projection of the noisy  $\tilde{\mathbf{v}} = \langle v\mathbf{1} + \mathbf{n} \rangle_{2\mathbf{venc}}$  to the closest line segment. Here, the “oblique projection” is determined by the  $\Sigma^{-1}(\mathbf{n})$  weighted distance. The search for the closest line segment is reduced to search for  $\mathbf{k} \in \mathcal{K}(\tilde{\mathbf{v}})$ .

### E. Conditional Distribution of the Estimate

In this section we derive  $\mathbb{P}(\hat{v}|v)$ , the distribution of the estimated velocity given the true velocity; this somewhat technical derivation in turn enables optimized design of  $\mathbf{venc}$  and the underlying first moments. To derive the distribution, we first establish two lemmas. The first lemma tells us that adding the same constant,  $\eta$ , to all noise realization components does not affect the error in detecting the wrapping integers and simply adds  $\eta$  to the PRoM velocity estimate, modulo  $\Omega$ .

**Lemma 1.** For  $\eta \in \mathbb{R}$ , let  $\mathbf{n}' = \mathbf{n} + \eta\mathbf{1}$  and  $\tilde{\mathbf{v}}' = \langle v\mathbf{1} + \mathbf{n}' \rangle_{2\mathbf{venc}}$ . Then

$$\hat{v}(\tilde{\mathbf{v}}') = \langle \hat{v}(\tilde{\mathbf{v}}) + \eta \rangle_\Omega \quad (40)$$

$$\langle \mathbf{k}^*(\tilde{\mathbf{v}}) - \mathbf{k}(\tilde{\mathbf{v}}) \rangle_{\mathbf{h}} = \langle \mathbf{k}^*(\tilde{\mathbf{v}}') - \mathbf{k}(\tilde{\mathbf{v}}') \rangle_{\mathbf{h}}. \quad (41)$$

*Proof.* By (31), we have

$$\begin{aligned} d_{2\mathbf{venc}}(\tilde{\mathbf{v}}', (v + \eta)\mathbf{1}) &= d_{2\mathbf{venc}}(\langle \tilde{\mathbf{v}} + \eta\mathbf{1} \rangle_{2\mathbf{venc}}, (v + \eta)\mathbf{1}) \\ &= d_{2\mathbf{venc}}(\tilde{\mathbf{v}} + \eta\mathbf{1}, (v + \eta)\mathbf{1}) \\ &= d_{2\mathbf{venc}}(\tilde{\mathbf{v}}, v\mathbf{1}). \end{aligned}$$

Thus  $\mathcal{L}(\tilde{\mathbf{v}}, v) = \mathcal{L}(\tilde{\mathbf{v}}', v + \eta)$  and  $\hat{v}(\tilde{\mathbf{v}}') = \langle \hat{v}(\tilde{\mathbf{v}}) + \eta \rangle_\Omega$ . Below we compare estimates using  $\mathbf{k}^*$  versus the true  $\mathbf{k}$  along the  $\mathbf{1}$  direction. By (26)

$$\begin{aligned} &\langle \hat{v}(\tilde{\mathbf{v}}) - \mathbf{w}^\top (v\mathbf{1} + \mathbf{n}) \rangle_\Omega \\ &= \langle \mathbf{w}^\top (\langle \mathbf{k}^*(\tilde{\mathbf{v}}) - \mathbf{k}(\tilde{\mathbf{v}}) \rangle_{\mathbf{h}} \circ 2\mathbf{venc}) \rangle_\Omega, \end{aligned} \quad (42)$$

and

$$\begin{aligned} & \langle \widehat{\mathbf{v}}(\tilde{\mathbf{v}}') - \mathbf{w}^\top(v\mathbf{1} + \mathbf{n}') \rangle_\Omega \\ &= \langle \mathbf{w}^\top(\langle \mathbf{k}^*(\tilde{\mathbf{v}}') - \mathbf{k}(\tilde{\mathbf{v}}') \rangle_{\mathbf{h}} \circ 2\mathbf{venc}) \rangle_\Omega. \end{aligned} \quad (43)$$

By the previously derived  $\widehat{\mathbf{v}}(\tilde{\mathbf{v}}') = \langle \widehat{\mathbf{v}}(\tilde{\mathbf{v}}) + \eta \rangle_\Omega$ , so we have

$$\begin{aligned} & \langle \widehat{\mathbf{v}}(\tilde{\mathbf{v}}') - \mathbf{w}^\top(v\mathbf{1} + \mathbf{n}') \rangle_\Omega \\ &= \langle \widehat{\mathbf{v}}(\tilde{\mathbf{v}}) + \eta - \mathbf{w}^\top(v\mathbf{1} + \mathbf{n}) - \eta \rangle_\Omega \\ &= \langle \widehat{\mathbf{v}}(\tilde{\mathbf{v}}) - \mathbf{w}^\top(v\mathbf{1} + \mathbf{n}) \rangle_\Omega. \end{aligned}$$

Thus (42) and (43) are equal for all  $\mathbf{w}$ , and

$$\langle \mathbf{k}^*(\tilde{\mathbf{v}}) - \mathbf{k}(\tilde{\mathbf{v}}) \rangle_{\mathbf{h}} = \langle \mathbf{k}^*(\tilde{\mathbf{v}}') - \mathbf{k}(\tilde{\mathbf{v}}') \rangle_{\mathbf{h}}. \quad \square$$

Fig. 4 provides visualisation of wrapping integers  $\mathbf{k}^*(\tilde{\mathbf{v}})$  for the case  $\mathbf{venc} = [35, 10, 14]^\top$ ,  $[s_{11}, s_{21}, s_{31}] = [2.5, 5, 2.5]$ . All  $\tilde{\mathbf{v}}$  along direction  $\mathbf{1}$  inside the hyper-rectangle share the same  $\mathbf{k}^*$ , which is a consequence of Lemma 1.

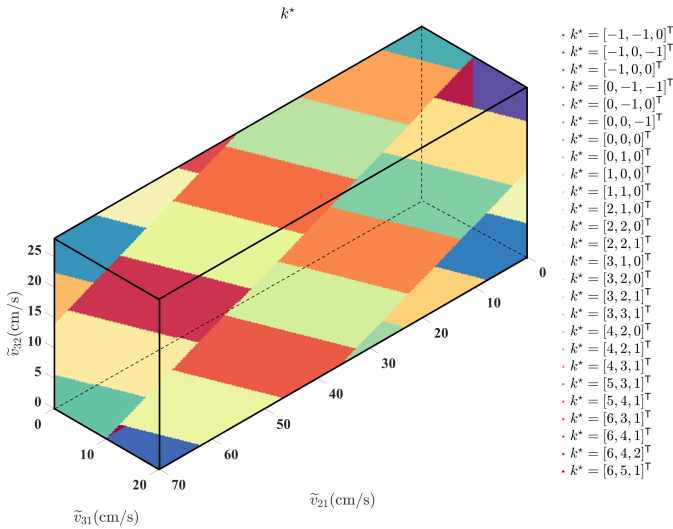


Fig. 4. Illustration of wrapping integers  $\mathbf{k}^*(\tilde{\mathbf{v}})$ ,  $N_c = 1$ ,  $N_e = 3$ ,  $\mathbf{venc} = [35, 10, 14]^\top$ ,  $[s_{11}, s_{21}, s_{31}] = [2.5, 5, 2.5]$ . The colored tiles for each region are drawn on the surfaces of the hyper-rectangle, and regions extend unchanged parallel to the  $[1, 1, 1]^\top$  direction, which is the direction of the line of sight in the figure. PRoM detects wrapping integers for fast, accurate estimation of velocity.

In addition,  $\mathcal{L}(\tilde{\mathbf{v}}, v_k)$  as a function of  $\tilde{\mathbf{v}}$  is piece-wise quadratic with the same curvature for all  $\mathbf{k}$ , so the decision boundaries of  $\mathbf{k}^*(\tilde{\mathbf{v}})$  are linear, which is also illustrated in Fig. 4.

By Lemma 1, the error in wrapping integers,  $\langle \mathbf{k}^*(\tilde{\mathbf{v}}) - \mathbf{k}(\tilde{\mathbf{v}}) \rangle_{\mathbf{h}}$ , remains constant for all noise realizations  $\mathbf{n}$  along any line parallel to  $\mathbf{1}$ . So, we can divide the space of all possible noise realizations,  $\mathbb{R}^{\frac{N_e(N_e-1)}{2}}$ , into “tubes”  $\mathcal{T}(\mathbf{x})$  parallel to  $\mathbf{1}$ , based on the difference,  $\mathbf{x}$ , of estimated wrapping integers  $\mathbf{k}^*$  and true wrapping integers  $\mathbf{k}$ .

$$\mathcal{T}(\mathbf{x}) = \{\mathbf{n} | \langle \mathbf{k}^*(\tilde{\mathbf{v}}) - \mathbf{k}(\tilde{\mathbf{v}}) \rangle_{\mathbf{h}} = \mathbf{x}\}. \quad (44)$$

We can, as seen below, integrate over these tubes to arrive at error probabilities for detecting the wrapping integers. Next we

establish a second lemma describing the orthogonality between pairwise noise differences and the error in the estimated velocity.

**Lemma 2.**

$$n_{ab} - n_{cd} \perp \mathbf{w}^\top \mathbf{n}, ab \neq cd \quad (45)$$

*Proof.*

$$\begin{aligned} & \text{cov}(\mathbf{w}^\top \mathbf{n}, n_{ab} - n_{cd}) \\ &= \mathbf{w}^\top \mathbb{E}(\mathbf{n}(n_{ab} - n_{cd})) \\ &= \frac{\mathbf{1}^\top \Sigma^{-1}(\mathbf{n}) \Sigma(\mathbf{n}) (\mathbf{e}_{ab} - \mathbf{e}_{cd})}{\mathbf{1}^\top \Sigma(\mathbf{n})^{-1} \mathbf{1}} = 0, \end{aligned}$$

where  $\mathbf{e}_{ab}$  is the standard basis equal to 1 at one position corresponding to  $n_{ab}$  in  $\mathbf{n}$ , and 0 otherwise.  $\square$

Armed with the two lemmas, we can specify the distribution.

**Theorem 1.** Given  $v$ ,  $\forall \mathbf{n} \in \mathcal{T}(\mathbf{x})$ ,  $\widehat{\mathbf{v}}(\tilde{\mathbf{v}})$  follows wrapped normal distribution  $\mathcal{N}(\langle v + \mathbf{w}^\top(\mathbf{x} \circ 2\mathbf{venc}) \rangle_\Omega, \mathbf{w}^\top \Sigma(\mathbf{n}) \mathbf{w})$ .

*Proof.* Note that the event  $\mathbf{n} \in \mathcal{T}(\mathbf{x})$  is only determined by the pairwise difference of  $n_{ab} - n_{cd}$  thus uncorrelated, thereby independent of  $\mathbf{w}^\top \mathbf{n}$  by the Gaussian assumption (25). So, for all  $\mathbf{n} \in \mathcal{T}(\mathbf{x})$

$$\begin{aligned} \widehat{\mathbf{v}}(\tilde{\mathbf{v}}) &= \langle \mathbf{w}^\top(v\mathbf{1} + \mathbf{x} \circ 2\mathbf{venc} + \mathbf{n}) \rangle_\Omega \\ &= \langle v + \mathbf{w}^\top(\mathbf{x} \circ 2\mathbf{venc}) + \mathbf{w}^\top \mathbf{n} \rangle_\Omega. \end{aligned} \quad \square$$

Let  $f(\widehat{\mathbf{v}}|\mathcal{T}(\mathbf{x}), v)$  denote the conditional Gaussian probability density function (pdf) in Theorem 1 without wrapping by modulo  $\Omega$ . Thus, by wrapping the pdf function and invoking the law of total probability, we have

$$\mathbb{P}(\widehat{\mathbf{v}}|v) = \sum_{\mathbf{x}} \mathbb{P}(\mathbf{n} \in \mathcal{T}(\mathbf{x})|v) f_\Omega(\widehat{\mathbf{v}}|\mathcal{T}(\mathbf{x}), v) \quad (46)$$

$$f_\Omega(\widehat{\mathbf{v}}|\mathcal{T}(\mathbf{x}), v) = \begin{cases} \sum_{l \in \mathbb{Z}} f(\widehat{\mathbf{v}} + l\Omega|\mathcal{T}(\mathbf{x}), v), & \widehat{\mathbf{v}} \in [0, \Omega) \\ 0, & \text{otherwise} \end{cases}$$

To complete (46), we need only to calculate  $\mathbb{P}(\mathbf{n} \in \mathcal{T}(\mathbf{x})|v)$  by integration of a multivariate normal distribution. Leveraging Lemma 1, the integration can be simplified to a definite integration of a normal distribution in  $\frac{N_e(N_e-1)}{2} - 1$  variables.

Fig. 5 illustrates the histogram of  $\widehat{\mathbf{v}}|v = 0$  using  $10^5$  trials,  $N_e = 3$ ,  $N_c = 1$ ,  $\mathbf{venc} = [99, 18, 22]^\top$  cm/s at  $s_{21} = 5, 10$ . Invoking Theorem 1, we predict the five most probable wrapping integers, which correspond to detection regions  $\mathcal{T}([0, 0, 0]^\top)$ ,  $\mathcal{T}([5, 4, 1]^\top)$ ,  $\mathcal{T}([6, 5, 1]^\top)$ ,  $\mathcal{T}([1, 1, 0]^\top)$ , and  $\mathcal{T}([10, 8, 2]^\top)$ . These five predicted detections correspond to  $f(\widehat{\mathbf{v}}|\mathcal{T}(\mathbf{x}), v)$  centered at 0 (the true velocity),  $\pm 177.81$ , and  $\pm 40.37$  cm/s; these five predictions are validated in the histogram. For the higher SNR case of  $s_{21} = 10$ , the probability of unwrapping errors goes very small, and the  $10^5$  trials are insufficient to encounter an unwrapping error to  $\pm 40.37$  cm/s.

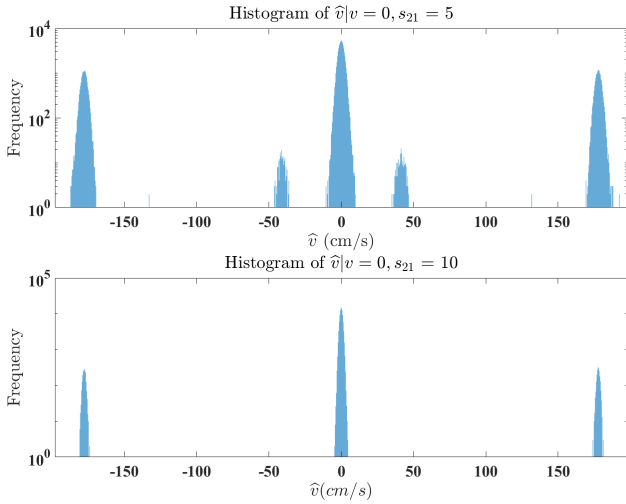


Fig. 5. Histogram from  $10^5$  trials of  $\hat{v}|v = 0$ , for  $N_c = 1$ ,  $N_e = 3$ ,  $\mathbf{venc} = [99, 18, 22]^T$  cm/s,  $v = 0$ , at  $s_{21} = 5$  (top) and  $s_{21} = 10$  (bottom).  $2s_{11} = s_{21} = 2s_{31}$ . Note the logarithmic scale for the vertical axis covering four (top) and five (bottom) orders of magnitude. The histogram illustrates both noise sensitivity via the spread of each Gaussian component and the probability of unwrapping errors via the presence of multiple components.

### F. Three-point Encoding

We consider here three-point encoding for velocity in one direction. Due to (9, 14), every  $\text{venc}_{ab}$ , and hence the unambiguous range,  $\Omega$ , depends only on the differences between first moments; thus,  $\text{venc}_{ab}$  and  $\Omega$  are unaffected by adding the same constant to every first moment. We assume the following ordering for the first moments:

$$m_{11} < m_{12} < m_{13}, m_{12} - m_{11} < m_{13} - m_{11}. \quad (47)$$

Thus, the three  $\text{venc}$ s are ordered:  $\text{venc}_{31} < \text{venc}_{32} < \text{venc}_{21}$ . Let  $\xi = \frac{\text{venc}_{32}}{\text{venc}_{31}}$ , noting that (9) and (47) imply  $\xi \in (1, 2)$ . For rational  $\xi = p/q$  with co-prime integers  $p$  and  $q$ , the unambiguous range  $\Omega$  in (14) is

$$\Omega = 2(p - q)\text{venc}_{21}. \quad (48)$$

Thus, by jointly unwrapping multiple  $\text{venc}$ s one can construct an unaliased velocity range that is larger than the highest  $\text{venc}$ ,  $\text{venc}_{21}$ , by a factor of  $2(p - q)$ . The covariance matrix for three-point encoding can be formulated via (24). Correspondingly, we can calculate the combination weights  $\mathbf{w}$  and the resulting RMSE given wrapping integers (26, 27). Armed with the explicit error variance and the probability of unwrapping errors derived below, we present in II-H an optimized design of  $\mathbf{venc}$  for three-point encoding with the constraint on the largest first moment, given a desired unambiguous range of velocities to be observed and SNR level for each encoding.

### G. Existing Estimators for Three-point Encoding

In the notation of (10) and (13), the approaches in [3], [4] use the unaliased high  $\text{venc}$  measurement,  $\tilde{v}_{21}$ , to unwrap the low  $\text{venc}$  measurement,  $\tilde{v}_{31}$ , while  $\text{venc}_{32}$  goes unused.

The estimator in [4], which we denote as *standard dual-venc* (SDV), is given by

$$\hat{v} = \begin{cases} \tilde{v}_{21} - 4\text{venc}_{31}, & \frac{\tilde{v}_{21} - \tilde{v}_{31}}{2\text{venc}_{31}} \in (-2.4, -1.6) \\ \tilde{v}_{21} - 2\text{venc}_{31}, & \frac{\tilde{v}_{21} - \tilde{v}_{31}}{2\text{venc}_{31}} \in (-1.2, -0.8) \\ \tilde{v}_{21} + 2\text{venc}_{31}, & \frac{\tilde{v}_{21} - \tilde{v}_{31}}{2\text{venc}_{31}} \in (0.8, 1.2) \\ \tilde{v}_{21} + 4\text{venc}_{31}, & \frac{\tilde{v}_{21} - \tilde{v}_{31}}{2\text{venc}_{31}} \in (1.6, 2.4). \end{cases} \quad (49)$$

In [7], two potentially aliased measurements  $\tilde{v}_{31}, \tilde{v}_{32}$  are jointly unwrapped by minimizing

$$\hat{v} = \underset{v \in [-\Omega/2, \Omega/2]}{\text{argmin}} \sum_{l=(31,32)} \left( 1 - \cos \left( \frac{\pi v}{\text{venc}_l} - \tilde{\theta}_l \right) \right). \quad (50)$$

The authors dub their approach *optimal dual-venc* (ODV), and the minimization is accomplished by searching  $v \in [-\Omega/2, \Omega/2)$  with grid spacing  $\frac{\text{venc}_{31}}{1000}$ . The cost adopted in ODV is equivalent to

$$\frac{1}{2} \left| e^{i \frac{\pi v}{\text{venc}_{31}}} - e^{i \tilde{\theta}_{31}} \right|^2 + \frac{1}{2} \left| e^{i \frac{\pi v}{\text{venc}_{32}}} - e^{i \tilde{\theta}_{32}} \right|^2, \quad (51)$$

which intrinsically assumes no correlation between the noisy phase differences,  $\tilde{\theta}_{31}$  and  $\tilde{\theta}_{32}$ . The ODV approach recommends  $\text{venc}_{32} = \frac{3}{2}\text{venc}_{31}$ , yielding an unambiguous velocity range of length  $2\text{venc}_{21}$ , which is twice the highest  $\text{venc}$ . The choice  $\frac{3}{2}$  is a heuristic to lessen the probability of unwrapping errors when minimizing (50) in the presence of noise.

The non-convex optimization in [6] iteratively minimizes a cost similar to (51) with weights to accommodate a lower SNR in presence of intravoxel dephasing:

$$|\tilde{r}_{31}|^2 \left| e^{i \frac{\pi v}{\text{venc}_{31}}} - e^{i \tilde{\theta}_{31}} \right|^2 + |\tilde{r}_{32}|^2 \left| e^{i \frac{\pi v}{\text{venc}_{32}}} - e^{i \tilde{\theta}_{32}} \right|^2. \quad (52)$$

Both ODV and NCO can be applied to any number of encodings; further, the NCO algorithm also incorporates a spatial regularization across voxels in the form of the Laplacian of the velocity map.

### H. Design for Three-point Encoding

The selection of the pair  $\{\text{venc}_{31}, \xi\}$  defines first moments  $[m_{11}, m_{12}, m_{13}]$  up to translation. To minimize the worst intravoxel dephasing, we choose symmetric encoding  $m_{11} = -m_{13}$ ; to further ameliorate intravoxel dephasing, we allow for a user-defined upper bound on the largest first moment,  $m_{13} \leq m_\tau$ . The choice of  $\mathbf{venc}$  entails the interplay of noise sensitivity, probability of correct unwrapping, and the range of reliably unaliased velocities. We adopt a performance guarantee strategy for navigating these competing objectives. The design inputs are: the maximum range of velocities to be reliably detected,  $\Omega_\epsilon$ ; a lower bound of operating measurement SNR,  $s_{\alpha\beta}$ ; an upper bound,  $m_\tau$ , on the magnitude of the largest first moment; and, bounds on the per-pixel probability of an unwrapping error. The design outputs are the  $\mathbf{venc}$  and an underlying  $[m_{11}, m_{12}, m_{13}]$ . To formalize the notion of optimality, we make four definitions.

**Definition 1** (Unwrapping error). *If  $\langle \mathbf{k}^*(\tilde{\mathbf{v}}) - \mathbf{k}(\tilde{\mathbf{v}}) \rangle_h \neq \mathbf{0}$ , i.e., wrapping integers are incorrectly detected, then we say an Unwrapping Error occurs.*

**Definition 2** (Aliasing error). *Given no unwrapping error, if  $\hat{v}_{k^*}$  is aliased, then we say an Aliasing Error occurs.*

**Definition 3** ( $\epsilon$ -Reliable Range). *For given measurement SNR,  $s_{\alpha\beta}$ , and two small numbers  $\epsilon_1, \epsilon_2$ , the  $\epsilon$ -reliable range  $\Omega_\epsilon$  is the range of the velocities for which  $\mathbb{P}(\text{Unwrapping Error}) \leq \epsilon_1$  and  $\mathbb{P}(\text{Aliasing Error}) \leq \epsilon_2$ .*

Definition 3 allows us to specify a reliable velocity range  $\Omega_\epsilon < \Omega$  to guard against aliasing. Armed with these three definitions, we can now state a precise meaning of optimality for three-point design.

**Definition 4** (Optimal **venc** Design). *Given the SNR for the complex-valued data  $s_{\alpha\beta}$ , the desired maximum velocity range of length  $\Omega_\epsilon$ , an upper bound  $m_\tau$  on the largest first moment, and unwrapping error bounds  $\epsilon_1, \epsilon_2$ , the optimal **venc** minimizes the RMSE among all designs for which the unwrapping and aliasing errors satisfy  $\mathbb{P}(\text{Unwrapping Error}) \leq \epsilon_1$  and  $\mathbb{P}(\text{Aliasing Error}) \leq \epsilon_2$  across the entire range of length  $\Omega_\epsilon$ .*

Given  $s_{\alpha\beta}$  and **venc**,  $\mathbb{P}(\text{Unwrapping Error})$  can be calculated through Monte Carlo simulation by setting  $v = 0$  and counting the trials for which  $\langle \mathbf{k}^* - \mathbf{k} \rangle_h \neq \mathbf{0}$ . Independence of  $\mathcal{T}(\mathbf{x})$  on  $v$  allows simulation of  $v = 0$  to be sufficient. The number of trials is selected as  $100/\epsilon_1$  [16].

Bounding the Aliasing Error can be achieved via explicitly designing  $\Omega$  different than  $\Omega_\epsilon$ . Let the normal cumulative distribution function be  $\Phi(\cdot)$ . Then,  $\mathbb{P}(\text{Aliasing Error}) \leq \epsilon_2$  when

$$\Omega - \Omega_\epsilon \geq 2\Phi^{-1}(1 - \epsilon_2)\sqrt{\mathbf{w}^\top \Sigma(\mathbf{n}) \mathbf{w}}. \quad (53)$$

The design procedure in Alg. 2 is an offline finite search to optimally design **venc** and the corresponding first moments. To explore design options for  $\xi \in (1, 2)$ , we search rational values  $\xi = p/q$  among

$$\left\{ \frac{p}{q} \mid \text{gcd}(p, q) = 1, \frac{p}{q} \in (1, 2), p \leq P, q \leq Q \right\}, \quad (54)$$

where  $\text{gcd}(\cdot, \cdot)$  is greatest common divisor, and  $P, Q \in \mathbb{Z}^+$  are predefined upper bounds on the positive integers  $p, q$ .

The output  $[m_{11}, m_{12}, m_{13}]$  of Alg. 2 is a symmetric encoding that can be translated by  $\pm m_{13}$  to yield a referenced encoding; however, the referenced encoding suffers an increased risk of severe intravoxel dephasing, owing to the doubling of the largest first moment.

### III. METHODS

#### A. Simulation

To validate the two assumptions (25, 29) used in PRoM, we compare the RMSE for PRoM, the RMSE for grid search MLE, and the square root of the Cramér-Rao lower bound (CRLB) [11, p. 364] derived from complex measurements in (3). Results are computed for **venc** =  $[15, 6, 10]^\top$  cm/s and 50% intravoxel dephasing of amplitudes for high first moments:  $2s_{11} = s_{21} = 2s_{31}$ . RMSE values for both the MLE from the complex measurements and PRoM are each calculated using  $10^5$  trials, where the grid search of MLE on  $v$  has spacing 0.006 cm/s to avoid bias from gridding.

#### Algorithm 2 PRoM Optimal Design for Three-Point Encoding

**Require:**  $P, Q, s_{\alpha\beta}, \Omega_\epsilon, \epsilon_1, \epsilon_2, m_\tau$

```

1:  $\sigma \leftarrow \infty, p \leftarrow 2$ 
2: while  $p \leq P$  do
3:    $q \leftarrow 1$ 
4:   while  $q \leq Q$  do
5:     if  $\text{gcd}(p, q) = 1$  and  $\frac{p}{q} \in (1, 2)$  then
6:        $v \leftarrow 0, \mathbf{venc} \leftarrow [pq, q(p-q), p(p-q)]$ .
7:       Simulate  $\tilde{\mathbf{v}}$  with  $100\epsilon_1^{-1}$  trials, apply PRoM.
8:       if (Frequency of  $\langle \mathbf{k}^*(\tilde{\mathbf{v}}) - \mathbf{k}(\tilde{\mathbf{v}}) \rangle_h \neq \mathbf{0}$ )  $< \epsilon_1$  then
9:          $c \leftarrow \frac{\Omega_\epsilon}{\Omega - 2\Phi^{-1}(1 - \epsilon_2)\sqrt{\mathbf{w}^\top \Sigma(\mathbf{n}) \mathbf{w}}}$ 
10:         $c \leftarrow \max \left[ c, \frac{\pi}{2\gamma m_\tau q(p-q)} \right]^\top$ 
11:        if  $c\sqrt{\mathbf{w}^\top \Sigma(\mathbf{n}) \mathbf{w}} \leq \sigma$  then
12:           $\mathbf{venc} \leftarrow c\mathbf{venc}, \sigma \leftarrow c\sqrt{\mathbf{w}^\top \Sigma(\mathbf{n}) \mathbf{w}}$ 
13:        end if
14:      end if
15:    end if
16:     $q \leftarrow q + 1$ 
17:  end while
18:   $p \leftarrow p + 1$ 
19: end while
20:  $m_{11} \leftarrow \frac{-\pi}{2\gamma \text{venc}_{31}}, m_{12} \leftarrow \frac{\pi}{2\gamma \text{venc}_{31}} - \frac{\pi}{\gamma \text{venc}_{32}}, m_{13} \leftarrow -m_{11}$ 
Ensure: venc,  $[m_{11}, m_{12}, m_{13}]$ 

```

To compare the performance of PRoM versus SDV and ODV, we process the same measurements using different estimators. Simulation parameters include: **venc** =  $[15, 6, 10]^\top$  cm/s,  $[s_{11}, s_{21}, s_{31}] = [10, 20, 10]$ ,  $N_c = 1$  coil. The ODV estimation algorithm uses  $\tilde{v}_{31}, \tilde{v}_{32}$ , while SDV uses  $\tilde{v}_{31}, \tilde{v}_{21}$ . We calculate RMSE averaged over  $10^5$  trials at each true  $v$  on  $[-30, 30]$  cm/s sampled every 0.1 cm/s.

To assess the optimized encoding design in Alg. 2, we set a required velocity range of  $[-150, 150]$  cm/s and compare two choices of symmetric three-point encoding. Simulation parameters include:  $N_c = 1$  coil,  $s_{21} = 20$ . ODV and SDV recommend  $\xi = \frac{3}{2}$  and specify the three **venc**s to be **venc** =  $[150, 50, 75]^\top$  cm/s. For PRoM, we assume intravoxel dephasing leads to  $[s_{11}, s_{21}, s_{31}] = [10, 20, 10]$ , other input includes  $[P, Q] = [10, 10], [\epsilon_1, \epsilon_2] = [10^{-7}, 10^{-7}], \Omega_\epsilon = 300$  cm/s,  $\gamma m_\tau = \frac{\pi}{50}$  s/cm. The design procedure in Alg. 2 results in **venc** =  $[153.7274, 25.6212, 30.7455]^\top$  cm/s. Because PRoM uses a 95.2% larger  $m_{13}$  thereby potentially leading to more intravoxel dephasing, we advantage ODV and SDV by assuming no intravoxel dephasing:  $[s_{11}, s_{21}, s_{31}] = [20, 20, 20]$ . We calculate RMSE averaged over  $10^5$  trials at each true  $v$  on  $[-150, 150]$  cm/s sampled every 0.5 cm/s.

To simulate the complex intravoxel dephasing and assess estimator performance in this case, we simulate vessels as in [6] with circularly symmetric parabolic velocity profiles. Parameters include: 0.1 mm<sup>3</sup> isotropic resolution and  $N_c = 1$  coil. The five vessels share the same peak velocity 60 cm/s but have different diameters of 5.5, 3.9, 3.2, 2.7, 2.4 mm. The proton density is set to be 30% in the background region and 50% in the static tissue region compared to that in the vessel regions. The complex signal is generated using

(3) with symmetric three-point encoding such that  $\mathbf{venc} = [60, 20, 30]^T$  cm/s. Regions of  $5 \times 5 \times 5$  voxels are merged into one to generate intravoxel dephasing and  $0.5 \text{ mm}^3$  isotropic resolution. Then we add i.i.d. white complex Gaussian noise to make the maximum  $s_{\alpha\beta}$  for all voxels in the vessel regions reach 30.

## B. Phantom

A phantom experiment allows for a controlled comparison of estimation performance. An agarose gel-filled cylindrical container is used to generate the MRI signal. An air-coupled propeller rotates the container. The rotational rate is counted with a photomicrosensor [17]. The phantom was scanned on a 1.5T scanner (Siemens MAGNETOM Avanto). The in-plane bottom to top velocity increases linearly with the distance from the center of the container. In this experiment, we encode the vertical component of the in-plane velocity, which ranges from  $-240$  to  $240$  cm/s, using symmetric a three-point acquisition. The acquisition parameters include:  $N_c = 16$  coils;  $\mathbf{venc} = [200, 100, \frac{500}{3}]^T$  cm/s; field-of-view (FOV)  $520 \times 260$  mm; flip angle  $5^\circ$ ; TR 4.38 ms; TE 2.66 ms; and, matrix size  $192 \times 125$ . There are 15 repeated acquisitions. We use the averaged k-space as a reference to calculate the RMSE and aliasing error for all voxels except the background region across 15 scans.

## C. In Vivo

An in vivo experiment is used to verify that PRoM can unwrap velocity on an interval  $\Omega$  larger than twice the largest  $\text{venc}_{21}$ , as claimed in (48). A healthy volunteer was scanned on a 3T scanner (Siemens MAGNETOM Vida). For the recruitment and consent of human subject used in this study, the ethical approval was given by an Internal Review Board (2005H0124) at The Ohio State University. The  $\text{venc}$  scouting scan showed the maximum absolute value of velocity to be above 90 cm/s and less than 100 cm/s. A breath-held,  $N_c = 30$  coils, symmetric three-point encoding PC-MRI dataset was collected, with the imaging plane intersecting both the ascending aorta and descending aorta; through-plane velocity was encoded. Other acquisition parameters include: FOV  $360 \times 270$  mm; flip angle  $15^\circ$ ; TR 5.56 ms; TE 3.69 ms; matrix size  $192 \times 108$ ; and, cardiac phases, 13. The three-point acquisition is designed using Alg. 2 for:  $[P, Q] = [10, 10]$ ,  $[s_{1\beta}, s_{2\beta}, s_{3\beta}] = [5, 10, 5]$ ,  $[\epsilon_1, \epsilon_2] = [10^{-6}, 10^{-6}]$ ,  $\Omega_\epsilon = 200$  cm/s,  $\gamma m_\tau = \frac{\pi}{40}$  s/cm. The design results in  $\xi = 5/3$  with highest first moment  $\frac{\pi}{\gamma m_{13}} = 42$  cm/s. Restricted by input precision number of the scanner interface,  $\mathbf{venc} = [52.5, 21, 35]^T$  cm/s; the resulting unambiguous range is  $\Omega = 210$  cm/s, which is double the range  $[-52.5, 52.5]$  cm/s of SDV processing.

# IV. RESULTS

## A. Simulation Results

Fig. 6 numerically explores the approximations adopted in PRoM. The square root of the CRLB is plotted versus  $s_{21}$  for the model in (3) and provides a lower bound on the RMSE for any unbiased estimator. The bound is from a local

analysis of the likelihood function, and thus optimistically does not consider unwrapping errors. Superimposed are the RMSE values for both the MLE from the complex measurements and PRoM. For low SNR, both estimators diverge from the bound due to unwrapping errors. Both the MLE and PRoM asymptotically coincide with  $\text{CRLB}^{0.5}$ . Moreover, throughout the entire range of noise powers considered, the RMSE difference between MLE and PRoM is negligible, hence justifying the characterization of PRoM as an approximate MLE and validating the assumptions adopted in the derivation of the PRoM estimator.

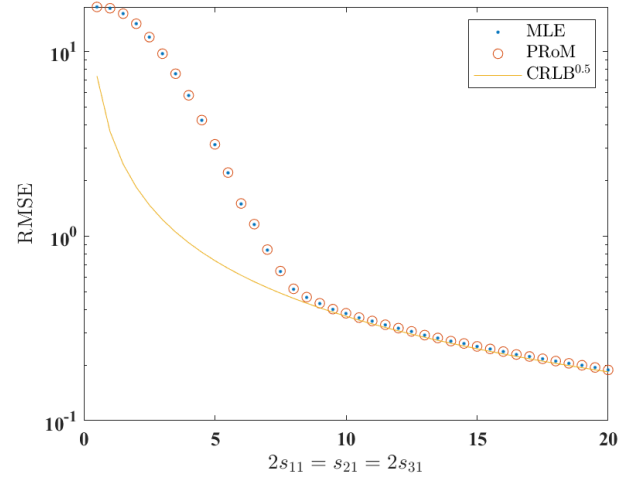


Fig. 6. Comparison of PRoM, the MLE directly from the complex-valued voxels, and  $\text{CRLB}^{0.5}$ . RMSE is graphed versus  $2s_{11} = s_{21} = 2s_{31}$ ; RMSE values for MLE and PRoM are averaged from  $10^5$  trials.

Fig. 7 shows the RMSE results for the same acquisition with  $10^5$  trials at each true velocity value with grid 0.1 cm/s. Both ODV and PRoM can unwrap a large range of velocities. The bottom panel zooms in to a smaller range of RMSE values; PRoM provides a small improvement in RMSE by modeling the non-zero noise covariance between phase difference measurements.

Fig. 8 shows the RMSE results for 1000 trials at each true velocity value with grid 0.1 cm/s. The SDV and ODV approaches share the same recommended acquisition strategy of  $\xi = \frac{3}{2}$ ; SDV computation uses  $\text{venc} = 50, 150$  cm/s whereas ODV jointly unwraps two phase differences from  $\text{venc} = 50, 75$  cm/s. Here we do a favor for ODV and SDV by assuming no intravoxel dephasing for their acquisition. For PRoM we assume intravoxel dephasing leads to  $2s_{11} = s_{21} = 2s_{31}$ . The PRoM design uses  $\xi = 6/5$ , which explicitly suppresses both Unwrapping Errors and Aliasing Errors to ensure reliable estimation across the full range,  $[-150, 150]$  cm/s. Further, despite the handicap of simulated 50% intravoxel dephasing, PRoM still provides a 10.5% decrease in RMSE compared to SDV and ODV used with their conventional acquisition strategy.

Figure. 9 shows the result for simulation of intravoxel dephasing. Panel (a) is the velocity profile simulated with refined resolution; (b) is the lower acquired resolution which leads to intravoxel dephasing. Panels (c), (d), (e) illustrate intravoxel dephasing for  $m_{11}, m_{12}, m_{13}$ . We observe more

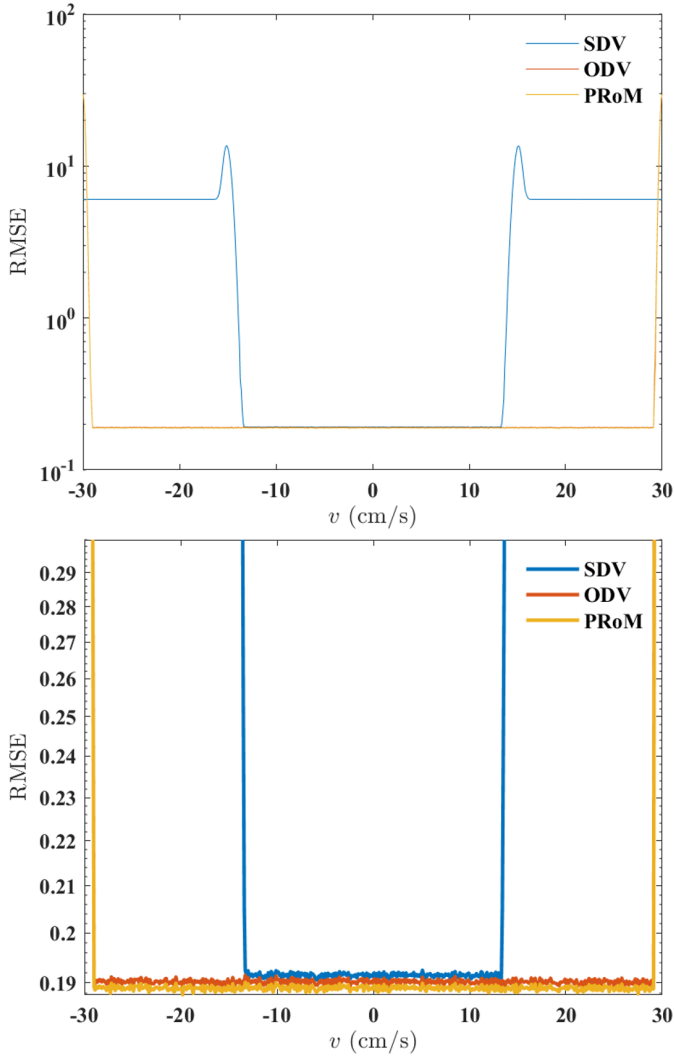


Fig. 7. Top: RMSE versus true  $v$  for  $\mathbf{venc} = [15, 6, 10]^T$  cm/s and  $[s_{11}, s_{21}, s_{31}] = [10, 20, 10]$ . RMSE values are averaged over  $10^5$  trials. Bottom: zoomed-in version.

serious intravoxel dephasing in  $m_{11}, m_{13}$  and at voxels close to the boundaries of the simulated vessels. Panels (f), (g), (h) show the recovered velocity. We can observe aliasing error in the SDV estimated velocity, but not in ODV and PRoM. Moreover, the RMSE given no Aliasing Error for SDV, ODV, and PRoM are 10.23, 10.24, and 10.12 cm/s, respectively.

### B. Phantom Results

Fig. 10 uses measured data from a healthy volunteer to validate that ODV and PRoM can unwrap a larger range of velocities than SVD, given the same encodings. The aliasing error ratio for SDV, ODV, and PRoM are  $1.716 \times 10^{-4}$ ,  $3.1777 \times 10^{-5}$ ,  $3.1777 \times 10^{-5}$ . The RMSE values given no aliasing error are 3.22, 3.60, 3.13 cm/s.

### C. In Vivo Results

From Fig. 11 panels (a), (b) and (c), we can observe more serious intravoxel dephasing for  $m_{11}, m_{13}$  compared to  $m_{12}$ .

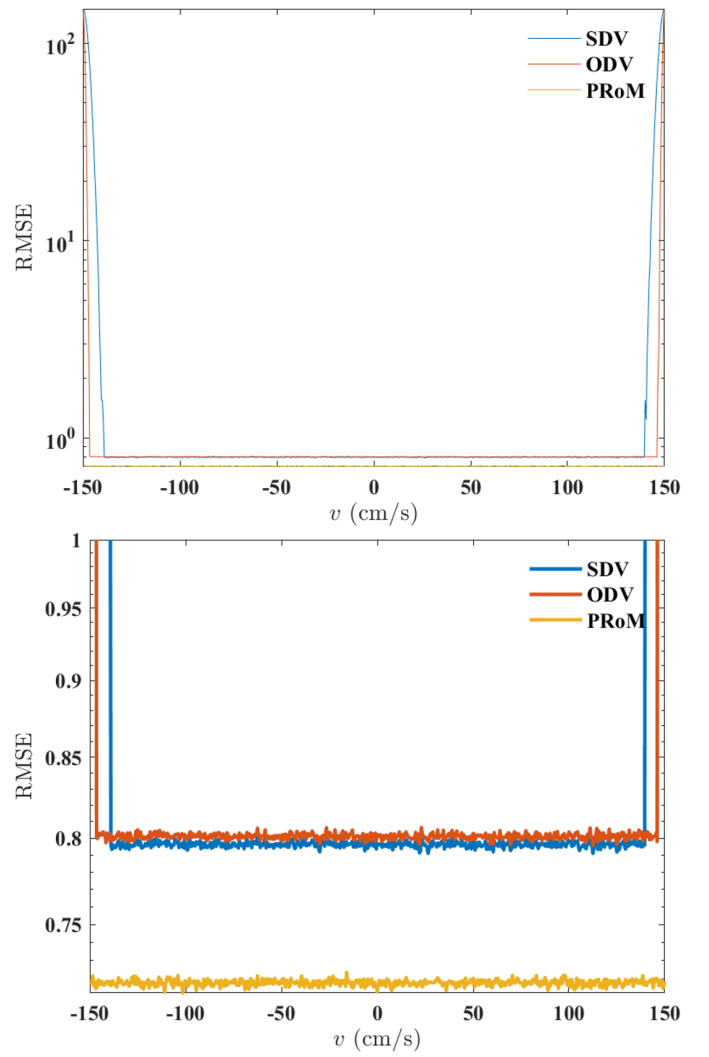
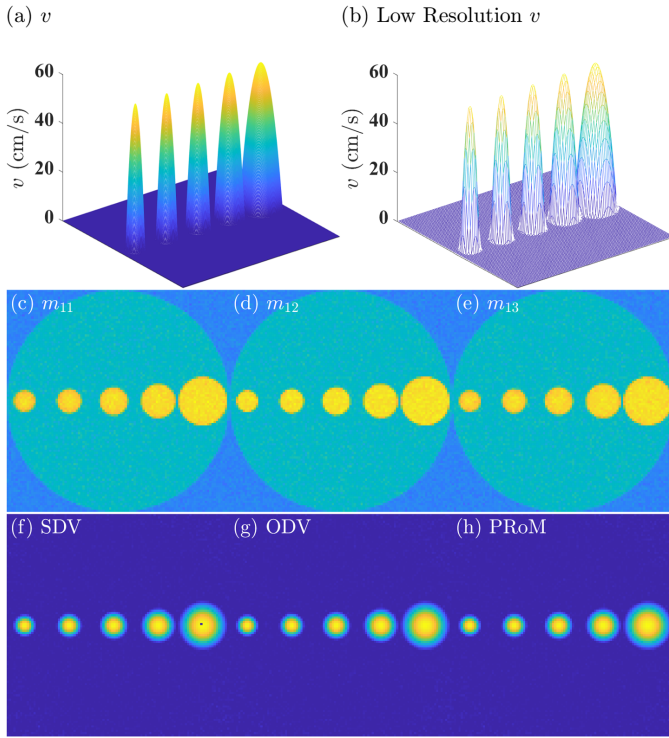


Fig. 8. Comparison of acquisition design and estimation for SDV, ODV, and PRoM: RMSE versus true velocity. Desired velocity range to be estimated is  $[-150, 150]$  cm/s. For SDV and ODV the three  $\mathbf{venc}$ s generated are  $\mathbf{venc} = [150, 50, 75]^T$  cm/s, whereas PRoM uses  $\mathbf{venc} = [153.7274, 25.6212, 30.7455]^T$  cm/s. Here we assume no intravoxel dephasing for ODV and SDV  $[s_{11}, s_{21}, s_{31}] = [20, 20, 20]$ . For PRoM we assume intravoxel dephasing and  $[s_{11}, s_{21}, s_{31}] = [10, 20, 10]$ . Top: RMSE versus true  $v$ . RMSE values are averaged over  $10^5$  trials. Bottom: zoomed-in version.

Because the largest absolute value of true velocity is larger than the largest  $\mathbf{venc}$  52.5 cm/s, we observe significant aliasing in SDV recovery from (d). However, (e) and (f) illustrate that both ODV and PRoM can recover velocities larger than the largest  $\mathbf{venc}$ . Here, the acquisition designed for PRoM departs from the  $\xi = 3/2$  heuristic to use  $\xi = 5/3$  and hence an unambiguous range of velocities four times that for standard dual- $\mathbf{venc}$  for the same highest  $\mathbf{venc}$ . Thus, the in vivo data illustrates the derivation in (48) and the associated design procedure in Alg. 2.

## V. DISCUSSION

The presentation here for PRoM is limited to a single component of velocity; extension to the estimation of all



**Fig. 9.** Comparison of SDV, ODV, and PRoM for simulated vessels.  $\mathbf{v}_{\text{enc}} = [60, 20, 30]^T$  cm/s. (a) is the true velocity profile. (b) is the lower acquisition resolution velocity profile. (c), (d), (e) are the magnitude images for  $m_{11}, m_{12}, m_{13}$ . (f), (g), (h) are the recovered velocities for SDV, ODV and PRoM.

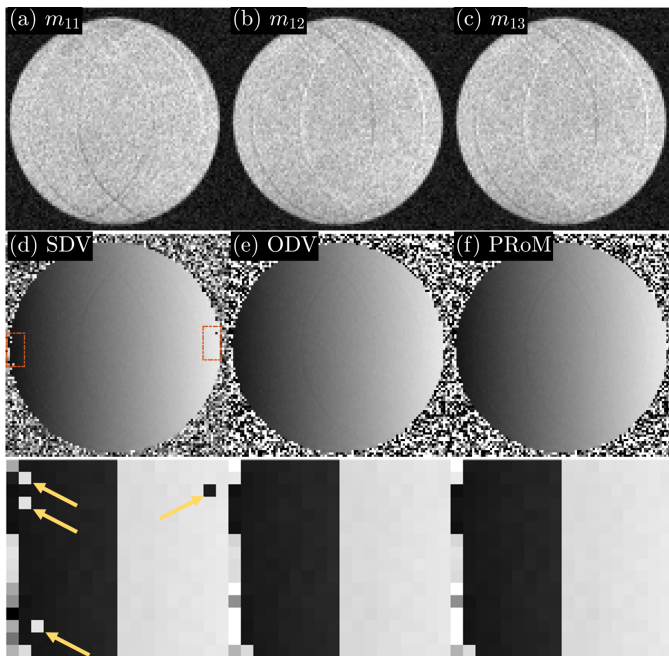


**Fig. 10.** Comparison of estimators for SDV, ODV, and PRoM.  $\mathbf{v}_{\text{enc}} = [250, 100, \frac{500}{3}]^T$  cm/s. The in-plane speed is within  $\pm 240$  cm/s.

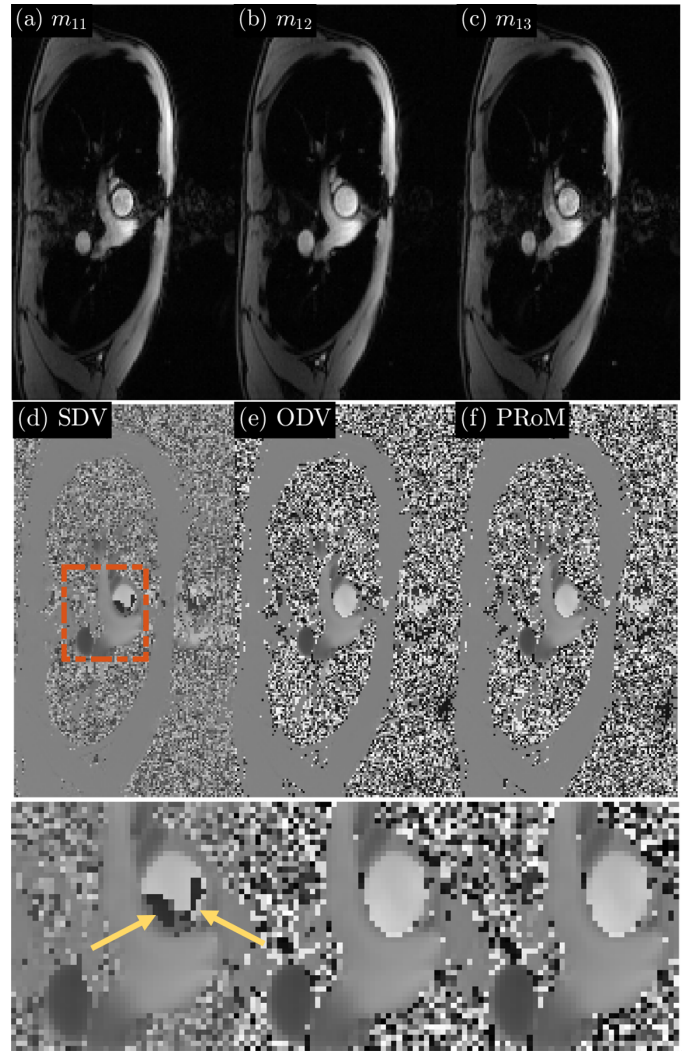


**Fig. 11.** Comparison for SDV, ODV, and PRoM velocity estimation for  $\mathbf{v}_{\text{enc}} = [52.5, 35, 21]^T$  cm/s. (a), (b), (c) are the square root of sum of squared coil images for  $m_{11}, m_{12}, m_{13}$ . (d), (e), (f) are the velocity estimates from SDV, ODV and PRoM. Bottom row are the zoomed-in versions of (d), (e), (f).

three velocity components, and hence congruence equations in multiple variables, is considered in [18]. Likewise, this presentation is restricted to voxel-by-voxel estimation of velocity. As noted in [6] for example, spatial correlations among velocities may be exploited to aid in the unwrapping of multiple encodings. In [6], this is accomplished using a Laplacian of the velocity map as a regularization term in a weighted least-squares fit the observed phase differences. Importantly, the conditional probabilities derived in II-E provide exact confidence values for the per-voxel unwrappings, as would be required for a principled Bayesian approach for spatial processing [19]. Spatial processing leveraging PRoM remains a topic for future investigation.

NCO [6] is a good estimator able to access the full unambiguous range of velocities; ODV [7] is a special case that assumes no phase variations due to intravoxel dephasing. However, NCO and ODV suffer three shortcomings relative to PRoM: computational complexity; assumption of a diagonal

covariance matrix that overlooks the inherent correlations among phase differences; and, no characterization of phase unwrapping probabilities. The MLE presented in (5) is itself a small contribution, extending array processing literature to the case of uncalibrated array gains; however, the MLE likewise is computationally complex and does not provide phase unwrapping probabilities.

The results in Fig. 11 illustrate that the PRoM-inspired design procedure in Alg. 2 can provide an unambiguous velocity range more than four times as large as the highest venc. Indeed, the design procedure in effect allows the range to grow to the greatest extent allowed by the presumed noise floor given as an input to the design. The design then minimizes the predicted RMSE while meeting constraints on unwrapping errors, reliable range of velocities, and maximum first moment. In the regime of very low SNR, the PRoM design yields  $\xi = 3/2$ , coinciding with the conventional heuristic [4], [7]. The Alg. 2 design provides unwrapping and velocity range guarantees, given a noise floor and bound on the highest first moment. For any higher SNR encountered, the guarantee still holds and the RMSE reduces according to (27).

Finally, for volumetric imaging applications with very large numbers of voxels, the processing speed of PRoM may provide a desirable benefit. The careful pruning of the set of candidate wrapping integers results in a fast estimator, without the need for expensive grid search nor gradient-based iterative optimization. Two orders of magnitude speed-up were observed for the in vivo example reported here.

## VI. CONCLUSION

In this work, we propose PRoM, an algorithm to solve a noisy set of linear congruence equations. We apply PRoM to single dimension velocity recovery in multi-coil phase-contrast MRI, with results presented for three-point acquisition. PRoM provides a fast approximate maximum likelihood estimator that fully leverages all pairwise phase differences while seamlessly accommodating coil combining and amplitude attenuation due to dephasing. PRoM can recover velocities across the full unambiguous range, which can be larger than twice the highest venc. Through PRoM, we can directly compute probabilities of unwrapping errors, and thereby formulate the posterior probability distribution of the velocity estimate. This innovation, in turn, allows for the optimized design of the phase-encoded acquisition, guaranteeing minimum estimation error subject to user-defined constraints on desired velocity range, unwrapping errors, aliasing errors, and maximum first moment of the encoding gradient. Simulation, phantom, and in vivo results validate the benefits of fast computation, reduced estimation error, increased unambiguous velocity range, and optimized acquisition.

## VII. ACKNOWLEDGMENT

The authors thank Dr. Ning Jin and Siemens Healthineers for providing the phantom data. The authors also thank Dr. Yingmin Liu and Dr. Chong Chen for their assistance with pulse sequence modification and data acquisition.

## REFERENCES

- [1] N. J. Pelc, R. J. Herfkens, A. Shimakawa, D. R. Enzmann *et al.*, "Phase contrast cine magnetic resonance imaging," *Mag. Reson. Quarterly*, vol. 7, no. 4, pp. 229–254, 1991.
- [2] M. Markl, A. Frydrychowicz, S. Kozerke, M. Hope, and O. Wieben, "4d flow MRI," *Journal of Magnetic Resonance Imaging*, vol. 36, no. 5, pp. 1015–1036, 2012.
- [3] A. T. Lee, G. B. Pike, and N. Pelc, "Three-point phase-contrast velocity measurements with increased velocity-to-noise ratio," *Magn. Reson. Med.*, vol. 33, pp. 122–126, 1995.
- [4] S. Schnell *et al.*, "Accelerated dual-venic 4D flow MRI for neurovascular applications," *J. Magn. Reson. Imaging*, vol. 46, no. 1, pp. 102–114, 2017.
- [5] S. Zhao, L. C. Potter, N. Jin, Y. Liu, O. P. Simonetti, and R. Ahmad, "PC-MRI with phase recovery from multiple wrapped measurements (PRoM)," in *Proc. 26th ISMRM Meeting & Exhibition*, Paris, France, 2018, p. 0685.
- [6] M. Loecher and D. B. Ennis, "Velocity reconstruction with nonconvex optimization for low-velocity-encoding phase-contrast MRI," *Magnetic resonance in medicine*, vol. 80, no. 1, pp. 42–52, 2018.
- [7] H. Carrillo, A. Osses, S. Uribe, and C. Bertoglio, "Optimal dual-venic unwrapping in phase-contrast MRI," *IEEE Trans. Med. Imag.*, vol. 38, no. 5, pp. 1263–1270, 2019.
- [8] W. Wang, X. Li, W. Wang, and X.-G. Xia, "Maximum likelihood estimation based robust Chinese remainder theorem for real numbers and its fast algorithm," *IEEE Trans. Signal Process.*, vol. 63, no. 13, pp. 3317–3331, 2015.
- [9] M. Wang and A. Nehorai, "Coarrays, MUSIC, and the Cramér-Rao bound," *IEEE Trans. Signal Process.*, vol. 65, no. 4, pp. 933–946, 2017.
- [10] K. R. O'Brien, B. R. Cowan, M. Jain, R. A. Stewart, A. J. Kerr, and A. A. Young, "MRI phase contrast velocity and flow errors in turbulent stenotic jets," *Journal of Magn. Reson. Imaging*, vol. 28, no. 1, pp. 210–218, 2008.
- [11] P. Stoica and R. Moses, *Spectral Analysis of Signals*. Upper Saddle River, NJ: Prentice-Hall, 2005.
- [12] C. F. Van Loan and G. Golub, "Matrix computations (johns hopkins studies in mathematical sciences)," *Matrix Computations*, 1996.
- [13] N. O'Donoghue and J. M. Moura, "On the product of independent complex Gaussians," *IEEE Trans. Signal Process.*, vol. 60, no. 3, pp. 1050–1063, 2012.
- [14] P. R. Halmos, "Positive approximants of operators," *Indiana University Mathematics Journal*, vol. 21, no. 10, pp. 951–960, 1972.
- [15] W. Wang, X. Li, W. Wang, and X.-G. Xia, "Maximum likelihood estimation based robust Chinese remainder theorem for real numbers and its fast algorithm," *IEEE Trans. Signal Process.*, vol. 63, no. 13, pp. 3317–3331, 2015.
- [16] M. Jeruchim, "Techniques for estimating the bit error rate in the simulation of digital communication systems," *IEEE J. Sel. Areas Commun.*, vol. 2, no. 1, pp. 153–170, 1984.
- [17] A. Vali, S. Schmitter, L. Ma, S. Flassbeck, S. Schmidt, M. Markl, and S. Schnell, "Development of a rotation phantom for phase contrast MRI sequence validation and quality control," *Magn. Reson. Med.*, vol. 84, no. 6, pp. 3333–3341, 2020.
- [18] S. Zhao, R. Ahmad, and L. C. Potter, "Maximizing unambiguous velocity range in phase-contrast MRI with multipoint encoding," *arXiv preprint arXiv:2111.03990*, 2021.
- [19] S. S. Saquib, C. A. Bouman, and K. Sauer, "ML parameter estimation for markov random fields with applications to bayesian tomography," *IEEE Trans. on Image Processing*, vol. 7, no. 7, pp. 1029–1044, 1998.